

Atomistic study on tensile fracture of densified silica glass and its dependence on strain rate

Zhi-Qiang Hu(胡志强)[1], Jian-Li Shao(邵建立)[1,†], Yi-Fan Xie(谢轶凡)[2], and Yong Mei(梅勇)[1,3,‡]
Citation: Chin. Phys. B, 2020, 29 (**12**): 128101. DOI: 10.1088/1674-1056/abb3f2
Journal homepage: http://cpb.iphy.ac.cn; http://iopscience.iop.org/cpb

What follows is a list of articles you may be interested in

Atomistic study on tensile fracture of densified silica glass and its dependence on strain rate

Zhi-Qiang Hu(胡志强)[1], Jian-Li Shao(邵建立)[1,†], Yi-Fan Xie(谢轶凡)[2], and Yong Mei(梅勇)[1,3,‡]
Chin. Phys. B, 2020, 29 (**12**): 128101. DOI: 10.1088/1674-1056/abb3f2

Mechanical and microstructural response of densified silica glass under uniaxial compression: Atomistic simulations

Yi-Fan Xie(谢轶凡), Feng Feng(冯锋), Ying-Jun Li(李英骏), Zhi-Qiang Hu(胡志强), Jian-Li Shao(邵建立), Yong Mei(梅勇)
Chin. Phys. B, 2020, 29 (**10**): 108101. DOI: 10.1088/1674-1056/aba5fe

Effect of metal fluorides on chromium ions doped bismuth borate glasses for optical applications

L Haritha, K Chandra Sekhar, R Nagaraju, G Ramadevudu, Vasanth G Sathe, Md. Shareefuddin
Chin. Phys. B, 2019, 28 (**3**): 038101. DOI: 10.1088/1674-1056/28/3/038101

Influences of annealing on structural and compositional properties of Al_2O_3 thin films grown on 4H-SiC by atomic layer deposition

Li-Xin Tian(田丽欣), Feng Zhang(张峰), Zhan-Wei Shen(申占伟), Guo-Guo Yan(闫果果), Xing-Fang Liu(刘兴昉), Wan-Shun Zhao(赵万顺), Lei Wang(王雷), Guo-Sheng Sun(孙国胜), Yi-Ping Zeng(曾一平)
Chin. Phys. B, 2016, 25 (**12**): 128104. DOI: 10.1088/1674-1056/25/12/128104

Tunable thermoelectric properties in bended graphene nanoribbons

Chang-Ning Pan(潘长宁), Jun He(何军), Mao-Fa Fang(方卯发)
Chin. Phys. B, 2016, 25 (**7**): 078102. DOI: 10.1088/1674-1056/25/7/078102

Atomistic study on tensile fracture of densified silica glass and its dependence on strain rate*

Zhi-Qiang Hu(胡志强)[1], Jian-Li Shao(邵建立)[1,†], Yi-Fan Xie(谢轶凡)[2], and Yong Mei(梅勇)[1,3,‡]

[1] *State Key Laboratory of Explosion Science and Technology, Beijing Institute of Technology, Beijing* 100081, *China*
[2] *School of Science, China University of Mining and Technology, Beijing* 100083, *China*
[3] *Institute of Defense Engineering, AMS, PLA, Beijing* 100036, *China*

(Received 22 June 2020; revised manuscript received 19 July 2020; accepted manuscript online 1 September 2020)

Densification is a major feature of silica glass that has received widespread attention. This work investigates the fracture behavior of densified silica glass upon uniaxial tension based on atomistic simulations. It is shown that the tensile strength of the silica glass approximately experiences a parabolic reduction with the initial density, while the densified samples show a faster power growth with the increase of strain rate. Meanwhile, the fracture strain and strain energy increase significantly when the densification exceeds a certain threshold, but fracture strain tends to the same value and strain energy becomes closer for different densified samples at extreme high strain rate. Microscopic views indicate that all the cracks are formed by the aggregation of nanoscale voids. The transition from brittleness fracture to ductility fracture can be found with the increase of strain rate, as a few fracture cracks change into a network distribution of many small cracks. Strikingly, for the high densified sample, there appears an evident plastic flow before fracture, which leads to the crack number less than the normal silica glass at the high strain rate. Furthermore, the coordinated silicon analysis suggests that high strain rate tension will especially lead to the transition from 4- to 3-fold Si when the high densified sample is in plastic flow.

Keywords: silica glass, densification, fracture, strain rate, atomistic simulation

PACS: 81.05.Kf, 81.70.Bt, 62.20.mm, 62.20.–x **DOI:** 10.1088/1674-1056/abb3f2

1. Introduction

Nowadays, glass materials have been paid much attention due in part to their excellent mechanical properties.[1–4] As a widely used protective material, the fracture behavior of silica glass is very important. The silica glass is a well-known brittle material[5] in nature, which only needs to absorb a little energy during the fracture process.[6,7] In experiments, an atomic force microscope was used to characterize the fracture surfaces. It was proved that the cracks are formed by the growth, aggregation, and propagation of nanoscale voids[8] and the evolution of void is the key to the failure of materials.[9] The formation of these nanoscale voids is mainly due to the roughness of the material surface.[10] However, the required spatiotemporal resolutions for a comprehensive understanding of the nanoscale void nucleation and growth is still prohibitive for state-of-the-art experimental techniques.

As a powerful supplement to the experiment, molecular dynamics (MD) simulation[11] has been successfully applied in many microscopic mechanism studies in recent years. Based on MD simulations, Muralidharan *et al.*[12] obtained higher tensile strength by considering atomic charge transfer during the deformation of silica glass. Besides, they concluded that the strain rate below 10^9 s^{-1} has little effect on the tensile strength, and used 2-M ring to describe the formation mechanism of the voids systematically.[13] Except the qualitative mechanism description, the KIC value[14] of the silica is calculated directly from the atomic scale by means of the *J* integral,[15] which provides a new method to understand the fracture of the silica. Pedone *et al.*[16] shows that the critical value of fracture cavity is lower than the experimental value, which is considered to be the effect of size. The previous research has shown that the fracture behavior of the silica glass is influenced by various external factors, such as model size, quenching rate, temperature, and strain rate.[17–25] The tensile strength will increase rapidly to a plateau level when the strain rate exceeds 2.5×10^{11} s^{-1} and no more localization of damage in the sample. Importantly, the transition from brittleness to ductility was also observed with quenching rate and strain rate.

In addition to the external factors, the effect of densification on the fracture of silica glass is also worthy of attention. Yuan *et al.* obtained different densified silica glass by applying pressure at the quenching stage and they found that the void formation in densified silica glass has higher activation energy. Densified silica glass may display more plastic deformation before fracture due to the pre-existing cracks.[26] In essence, the densified silica glass is corresponding to the increase of coordination number of Si and O,[27] which can lead

*Project supported by Beijing Institute of Technology Research Fund Program for Young Scholars.
†Corresponding author. E-mail: shao_jianli@bit.edu.cn
‡Corresponding author. E-mail: meiyong1990@126.com
© 2020 Chinese Physical Society and IOP Publishing Ltd

to the tensile strength decrease.[28] The composition and function of different SiO_x ($x = 4$, 5, 6) structures are different in densified silica glass and this variation is often uneven.[29–31] Besides, the oxygen hexagonal close-packed (hcp) and face-centered cubic (fcc) clusters were also found in densified silica glass.[32] All these atomic structures are certain to affect the evolution and coalescence of voids. Thus, the fracture mechanism of densified silica glass has more physical implications.

To this day, there is still no comprehensive understanding of the fracture behavior of densified silica glass, although the fracture of normal silica glass has been deeply recognized. In this work, we examine the tensile fracture of densified silica glass based on atomistic simulations. The tensile strength and fracture mechanism of the different densified silica glass and their dependence on the strain rate are revealed by mechanical and microstructural analysis. The structure of manuscript is as follows: Model and simulation details are introduced in Section 2, results and discussion are presented in Section 3, and finally conclusion is drawn in Section 4.

2. Model and simulation details

2.1. Potential model

The BKS potential is a two-body potential based on the Buckingham potential with an added Coulombic term. Theoretical x-ray and neutron structure factors and effective neutron-weighted vibrational density of states of silica glass were computed by using a series of well-known interatomic potentials and compared to experimental results. It is found that the BKS potential was able to adequately reproduce both static structure and dynamical properties of silica glass.[33] Besides, the calculated values of the lattice constants, density, radial, and bond-angle distribution functions, equations of state, and phase transitions using different potentials are compared to experimental values. Simulation results with the BKS potential accurately predict the experimental measurements to within 2%.[34]

In this work, to avoid the possible unphysical effect at small interatomic distance, the modified BKS potential improved by Barmes *et al.*[35] is used, which has been used many times in the previous studies and can reproduce the structural and mechanical properties of silica glass[12,13,19,21,26] and densified silica glass.[31,32] The modified BKS potential is expressed as follows:

$$v = \begin{cases} \phi(r) = a_{ij}r^2 + b_{ij}r + c_{ij}, & r_{ij} \le r_{ij}^0, \\ v_{\mathrm{c}}^{\mathrm{BKS}}(r), & r_{ij}^0 < r_{ij} \le r_{\mathrm{c}}, \\ 0, & r_{ij} > r_{\mathrm{c}} \end{cases} \quad (1)$$

with

$$v_{\mathrm{c}}^{\mathrm{BKS}} = v^{\mathrm{BKS}}(r) - v^{\mathrm{BKS}}(r_{\mathrm{c}}) - (r - r_{\mathrm{c}})\frac{\mathrm{d}v^{\mathrm{BKS}}(r_{\mathrm{c}})}{\mathrm{d}r},$$

where a_{ij}, b_{ij}, and c_{ij} are parameters of $\phi(r)$. Here, we set $r_{\mathrm{c}} = 6.0$ Å, $r_{\mathrm{SiO}} = 1.5$ Å, and $r_{\mathrm{OO}} = 2.0$ Å.

2.2. Computational and analytical details

The preparation of samples and loading process are performed using LAMMPS.[36] The silica glass is prepared from crystalline silica by a quenching process. Firstly, a β-cristobalite (2.2 g/cm^3) containing 1022208 Si atoms and 2044416 O atoms is created and used as an initial structure. Then, different densified samples are obtained through four stages: melting, cooling, depressurizing, and relaxing stages. (i) The silica is melted at 6000 K for 200 ps under different pressures (0, 2, 4, 7, 10 GPa), ensuring that the memory of the silica crystal structure is completely removed. (ii) Cool the silica to room temperature, with the quenching rate of 57 K/ps. (iii) decompress the silica to zero pressure within 100 ps. (iv) Equilibrate the decompressed silica for 100 ps. The tensile tests are simulated in the strain rate range of 10^9 s^{-1}–10^{11} s^{-1} in NVE ensemble by uniformly changing the size of the simulated box along the Z direction. Periodic boundary conditions are applied in all the three directions.

The virial stress tensor[37] is calculated as follows:

$$\sigma_{\alpha\beta} = \frac{1}{V}\left(-\sum_i m_i v_{i\alpha} v_{i\beta} + \frac{1}{2}\sum_i \sum_{j\neq i} r_{ij\alpha} f_{ij\beta}\right), \quad (2)$$

where α and β represent x, y, and z coordinate axes, V is the volume of sample, m_i is the mass of atom i, $v_{i\alpha}$ and $v_{i\beta}$ indicate velocity of atom i along the coordinate axes α and β, respectively, $f_{ij\beta}$ represents force on the atom i triggered by atom j along the coordinate axis β, $r_{ij\alpha}$ represents distance between atoms i and j along the coordinate axis α. Note that the virial stress was already proved equivalent to the continuum Cauchy stress.[38]

The strain energy is calculated as follows:

$$U = V_0 \sum \int \sigma_i \mathrm{d}\varepsilon_i, \quad (3)$$

where V_0 is the volume of initial sample, i represents x, y, and z coordinate axes.

The local shear strain can be used to describe the plastic deformation on the atomistic level.[39,40] By comparing the current structure and a reference structure, the local deformation gradient transform matrix J_i can be determined as follows:

$$J_i = \left(\sum_{j\in N_i^0} d_{ji}^{0\mathrm{T}} d_{ji}^0\right)^{-1}\left(\sum_{j\in N_i^0} d_{ji}^{0\mathrm{T}} d_{ij}\right), \quad (4)$$

where d_{ij} is the separation (row) vector between atoms i and j (superscript 0 means the reference structure), atom j is one atom i's nearest neighbors, N_i^0 is the total number of nearest neighbors of atom i at reference structure.

The Green–Langrangian strain can be obtained by $\eta_i = \frac{1}{2}\left(J_i^{\mathrm{T}} J_i - I\right)$ and the local shear invariant strain[41] is calculated from matrix η_i:

$$\eta_i^{\text{miese}} = \sqrt{\left[\left(\eta_{xx}^i - \eta_{yy}^i\right)^2 + \left(\eta_{xx}^i - \eta_{zz}^i\right)^2 + \left(\eta_{yy}^i - \eta_{zz}^i\right)^2\right]/6 + \left(\eta_{xy}^i\right)^2 + \left(\eta_{xz}^i\right)^2 + \left(\eta_{yz}^i\right)^2}, \tag{5}$$

where η_{xx}^i, η_{yy}^i, η_{zz}^i, η_{xy}^i, η_{xz}^i, and η_{yz}^i are components of shear invariant strain at the atom i. Here, the calculation of η_i^{miese} for various atomic structure is performed using the software package OVITO.[42]

3. Results and discussion

3.1. Preparation of densified silica glass

In a small range, the atomic coordination of glass materials can be retained, resulting in a flawed and incomplete short-range ordered structure. The coordination states of five different densified (including normal density) silica glass samples are presented in Fig. 1(a), where the cutoff radius is 2.4 Å. It can be seen that the normal-coordinated silicon (4-fold Si) is dominant. With the increase of quenching pressure, 4-fold Si will gradually convert to over-coordinated silicon (such as 5-fold and 6-fold Si), which constitute the major defects in densified silica glass. When the quenching pressure reaches 10 GPa, the fraction of 5-fold Si in the sample is over 13%, and the fraction of 6-fold Si reaches about 0.5%, as reported in the literature.[26] Three different Si coordination groups are presented in Fig. 1(b), in which 4-fold Si, 5-fold Si, and 6-fold Si are marked by A, B, and C. In fact, the larger the coordination number is, the higher the density is.

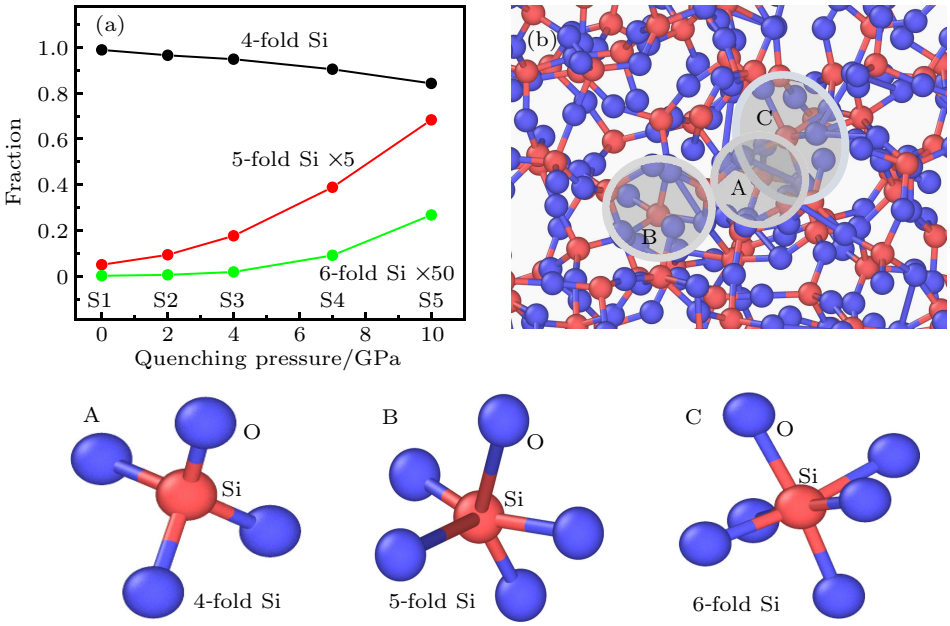


Fig. 1. (a) Fraction of different coordinated silicon samples *versus* quenching pressure. (b) Local amplified view of the atomic structures.

Table 1. Different silica glass models and strain rate modes.

Sample designation	Quenching pressure/GPa	Initial density/(g/cm^3)	Dimensions ($L_X \times L_Y \times L_Z$)/nm	Strain rate designation	Strain rate/s^{-1}
S1	0	2.20	31.39×31.39×47.09	SR1	10^9
S2	2	2.31	30.88×30.88×46.32	SR2	5×10^9
S3	4	2.41	30.46×30.46×45.69	SR3	10^{10}
S4	7	2.54	29.92×29.92×44.88	SR4	5×10^{10}
S5	10	2.66	29.46×29.46×44.19	SR5	10^{11}

3.2. Stress–strain relation and the tensile strength

The normal stress–strain and the shear stress–strain curves of S1, S3, and S5 at five strain rates (SR1–SR5) are plotted in Fig. 2, where the shear stress $\tau = [\sigma_{zz} - (\sigma_{xx} + \sigma_{yy})/2]/2$, the engineering strain $((V - V_0)/V_0)$ is adopted. When the strain rate is lower than SR3, we find that the stress in S1 and S3 decreases sharply to zero after reaching the peak value, showing a typical characteristic of brittleness fracture. The reason is that the atomic structure undergoes a similar rearrangement as the quasi-static tests. At higher strain rates (SR4 and SR5), the samples have not been completely fractured even if the strain reaches 50%, due to the transition from brittleness to ductility. In this case, the tensile nanoscale voids do not have enough time to further grow and merge into a big crack. As a result, there forms the damage region all over the sample. In addition, it is also observed that the fracture

strain (corresponding to the maximum stress) increases with the strain rate, indicating a gradual transformation process. Very interestingly, we observed a significant plastic flow phase before the complete fracture in high densified silica glass (S5) and the fracture strain exceeds 30% for all the strain rates. In other words, S5 needs absorbing more energy during the fracture and then shows a very different deformation failure. Besides, both S1 and S3 exhibit a phenomenon of bulk phase rebound with the rapid decrease of stress, but this phenomenon no more appears in S5 because of the significant plastic flow.

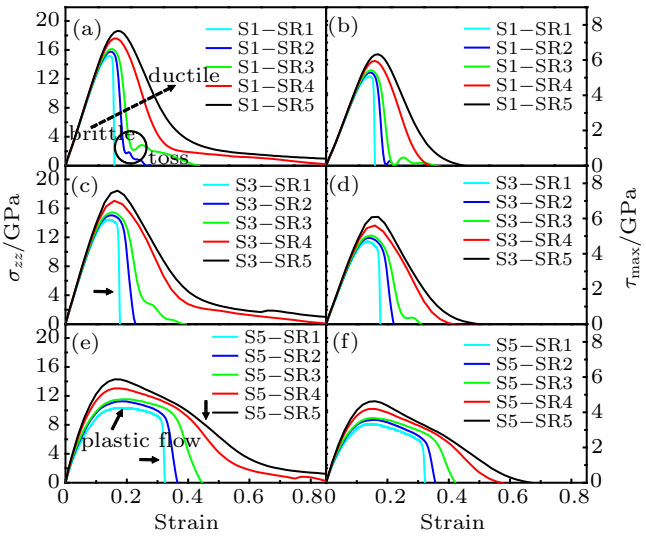


Fig. 2. Normal stress–strain [(a), (c), (e)] and shear stress–strain [(b), (d), (f)] curves of different types of densified silica glass at five different strain rates (SR1–SR5). The transition from brittleness fracture to ductility fracture with strain rate, and a significant plastic flow in the high densified sample are both shown.

The tensile strength as a function of densification and strain rate are plotted in Fig. 3. As for normal silica glass (S1), the tensile strength varies about from 15 GPa to 20 GPa with the increase of strain rate, which agrees well with other results based on BKS potential.[12,13] These results are somewhat higher than the experimental observations (11 GPa–14 GPa) at quasi-static loading[43] as expected. At SR1, we find that the tensile strength approximately undergoes a parabolic reduction ($f(x) = -121.6 + 122.4x - 27.4x^2$) with the initial density and that may depend on the accumulated activation energy by the densification.[26] Interestingly, the increase of strain rate will gradually change the variation law, and we can observe that the tensile strength of S2 becomes a little higher than S1 at SR5 (M point). For each densified sample, the variation with strain rate is consistent with other observations, satisfying the power law function. But, it is shown that the tensile strength of higher densified samples increases faster with the increase of strain rate. The power law for S1 and S5 can be written as $f(x) = 5.72x^{0.046}$ and $f(x) = 2.33x^{0.071}$, respectively, and the power law factor increases obviously with the increase of initial density. In fact, the elastic deformation occurs at the speed of sound, which is independent of the strain rate, while plastic deformation by a series of local plastic deformation aggregation[44,45] does not have enough time to occur at higher strain rates, which finally leads to the increase of the tensile strength macroscopically. In general, these results indicate that the tensile strength of the samples is influenced by the coupling of densification and strain rate.

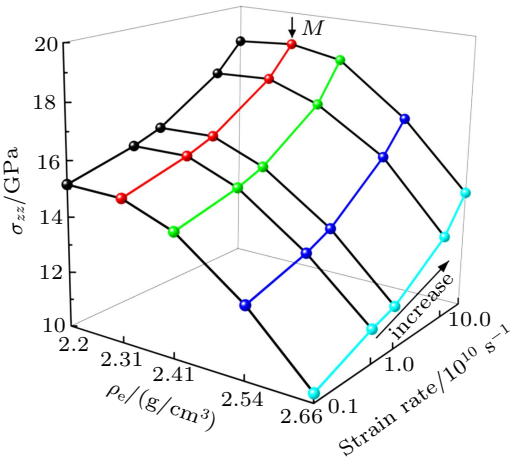


Fig. 3. Tensile strength of silica glass *versus* initial density and strain rate. The tensile strength reduces approximately with a parabolic function of the initial density, while the densified samples show a faster power increase with the strain rate.

Meanwhile, the variation of fracture strain is shown in Fig. 4(a). With the increase of strain rate, we find that the fracture strain of S1–S4 undergoes a similar increase. In particular, the fracture strain of S5 is much greater than others when the strain rate is lower than 10^{10} s^{-1} (SR3). In fact, the densification can exhibit evident effect until the density of silica glass reaches a critical value. We can observe that the fraction of over-coordinated Si of S5 is over 13% and more than other samples from Fig. 1. As shown in Fig. 4(b), we can see that the strain energy of S5 and other samples undergoes a similar increase and the strain energy of S5 is also much greater than others at all strain rates. It means that the fraction of dense atomic clusters[46–48] in structure of S5 is more than other samples. When the sample is deformed, the atoms of these regions need more energy to rearrange, which leads to the increasing of fracture strain. It can also be predicted that the deformation failure of high densified silica glass (S5) will be different from others. However, the fracture strains of S1–S4 converge to the same value at SR4 and the fracture strain of S5 begins a fast reduction after 10^{10} s^{-1} (SR3) and merges with others when the strain rate arrives at 10^{11} s^{-1} (SR5). It is shown that the strain at the maximum of stress cannot clearly describe differences of densified silica glass at high strain rate. In Fig. 4(b), the differences of strain energy of all samples become closer. It means that the fracture behavior of silica glass is sensitive to the high strain rate, which eventually masks the densification effect. In other words, the strain rate plays a more important role than densification at higher strain rate.

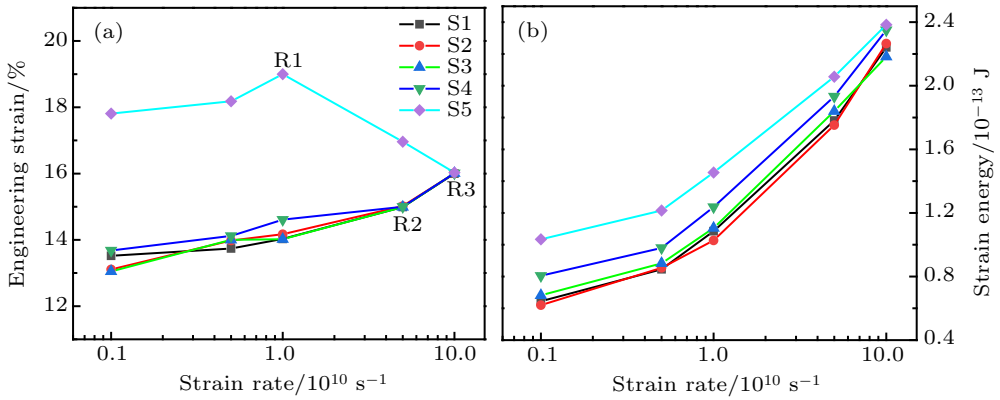


Fig. 4. Fracture strain of different types of densified silica glass *versus* strain rate (a). Strain energy of different densified silica glass *versus* strain rate (b). Here, the fracture strain denotes the strain at the maximum of stress.

3.3. Fracture mechanism of densified silica glass

The microscopic evolution of fracture in different densified silica glass is further discussed in this subsection. According to the above results, we chose the two samples (S1 and S5) at two strain rates (SR1 and SR5) to show the difference in fracture mechanism. Firstly, the local shear strain in normal density S1 is presented in Figs. 5(a) and 5(b). When the strain exceeds 14.5% at SR1 (a), the localization of deformation occurs and the main cracks are formed in the following evolution, as a result of the nucleation, growth and convergence of the nanoscale voids. At the strain of 15%, we can see the complete fracture of S1 along the main crack. With the occurrence of fracture, the shear deformation will be recovered to some extent due to the stress relaxation and this phenomenon depends on the generation and propagation of fracture wave, which is discussed in Fig. 6. As expected, there exists a large damage in S1 at SR5 (b) when the strain is over 20%, and a network distribution of cracks will form all over the sample. When the strain reaches 50%, the sample has still not broken completely and the area ratio of the cracked region at this time is about 0.72, indicating a typical ductility fracture.

However, the high densified sample (S5) shows significant differences in fracture pattern. First of all, the fracture strain is obviously lagging behind and a large amount of local shear deformation occur before the fracture, which lead to the plastic flow state (see Fig. 2(e)). Figures 5(c) and 5(d) present the microscopic views of local shear strain in sample S5. At SR1 (c), the damage region has been expanded form three main cracks in the following evolution. Finally, the micro-voids of one main crack grow and merge, resulting in complete fracture. When the strain is increased from 32% to 32.5%, the area ratio of damage region varies from about 0.75 about 0.68 with the damage localization. Except the main crack, some damage forms isolated voids and others will close. At SR5 (d), the damage region is obviously larger than S1, but the localization of these damages is more evident in the subsequent stretching process, which lead to less cracks in S5 than S1, showing different dependences on the strain rate.

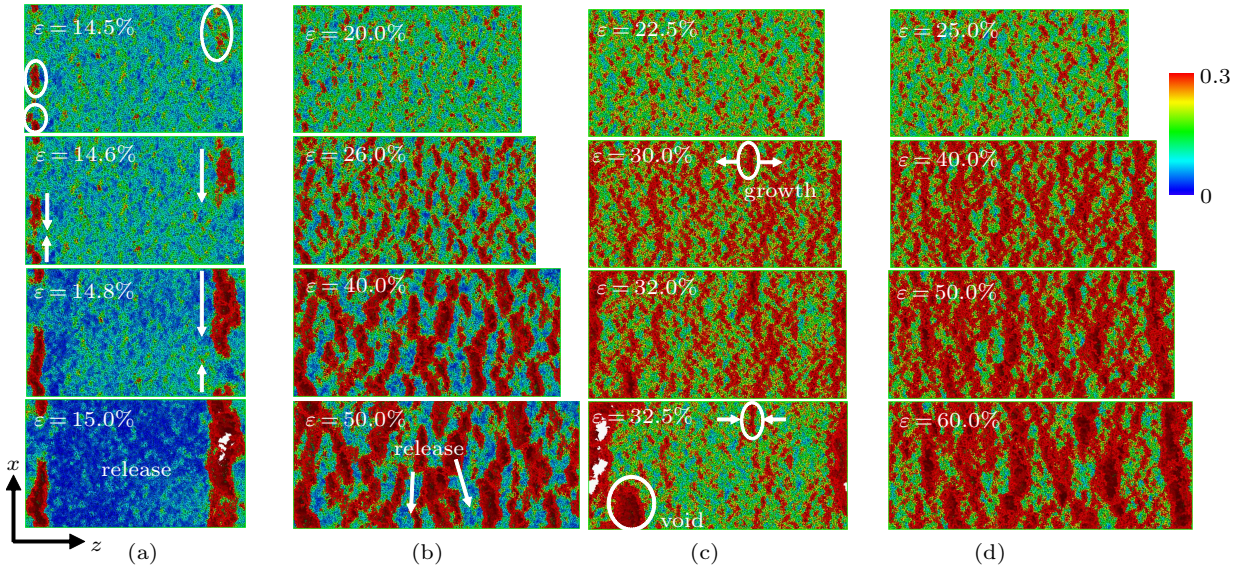


Fig. 5. Local shear strain evolution in S1 [(a), (b)] and S5 [(c), (d)] under uniaxial tension at SR1 [(a), (c)] and SR5 [(b), (d)]. The atoms are colored by the shear strain.

Based on the analysis of the microscopic process, we compare the stress profiles along the tensile direction between S1 and S5, and the results are shown in Fig. 6. When the fracture begins, the local stress rapidly approaches to zero. At the strain of SR1, with the evolution of local stress, we find obvious fracture waves in both S1 and S5. On both sides of the crack, the tensile stress will change to compressive stress because of the deformation relaxation. The peak value of compressive stress arrives at about −6.78 GPa and −4.12 GPa in S1 and S5, respectively. This indicates the release process of strain energy in addition to the formation of fracture plane. Thus, the rebound of bulk phase appears in the samples after complete fracture. While the high strain rate can only cause the overall reduction of stress in the sample. The tensile stress reduces to zero directly with very small fluctuations. As a result, the rebound of bulk phase is not observed at the strain rate of SR5.

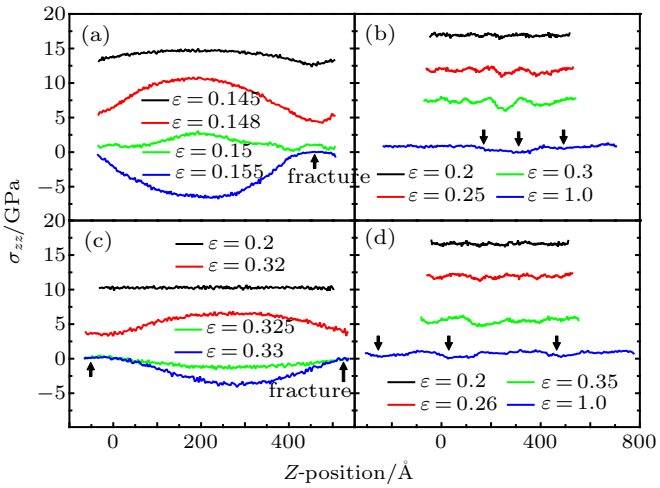


Fig. 6. The stress profiles of S1 [(a), (b)] and S5 [(c), (d)] at different strain rates [SR1: (a) and (c)]; SR5: (b) and (d).

Moreover, the radial distribution function (RDF), angular distribution function (ADF) and coordination number of S1 and S5 are analyzed to characterize the mechanism of atomic rearrangement during the uniaxial tensile tests of densified silica glass. The variation of Si–Si RDF at SR1 and SR5 are shown in Fig. 7. With increasing the strain, we firstly find the shift rightward of Si–Si peak of S1 (ε = 0–0.1) at SR1 (a), meaning that the Si–Si bonds elongate gradually. After fracture, the peak is recovered under the following tension (ε = 0.15–0.155) because of the stress relaxation. This process also appears at SR5 (b). For the high densified sample, we find the peak of S5 moves little to the right (ε = 0–0.2) at SR1 (c), implying the Si–Si bond is no more elongated obviously with the plastic flow. Only the shift leftward (ε = 0.2–0.325) after fracture is observed. This process also appears at SR5 (d). Also, there is a sudden increase of the peak at the high strain of SR5, indicating an increase in the number of nearest neighbors due to the strain rate effect. Besides, a small number of closer Si–Si bonds (new peak) are also observed.

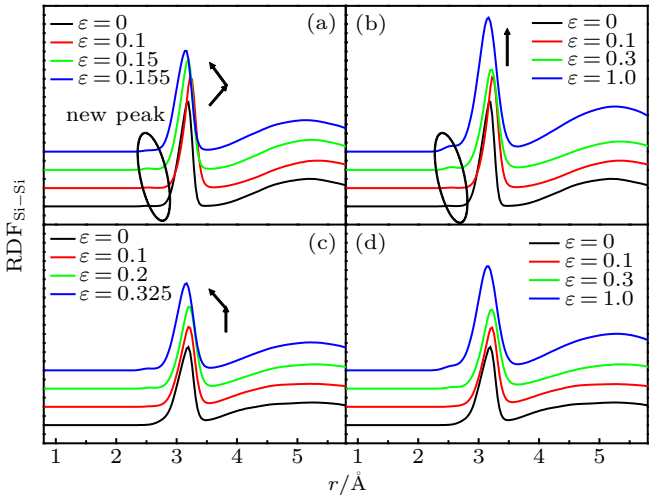


Fig. 7. The radial distribution function of Si–Si in S1 [(a), (b)] and S5 [(c), (d)] at different strain rates [SR1: (a) and (c); SR5: (c) and (d)]. The arrows indicate the change of the position of peak.

The Si–O–Si ADF at different strains is shown in Fig. 8. With the increase of strain, we find the peak of Si–O–Si angle in S1 shifts rightward to a larger value and then recovers, meaning that the Si–O–Si angle expansion before fracture and contraction after fracture. Besides, the new peak of Si–O–Si angle (called 2-M ring) can be observed. The plastic deformation mechanism of free volume model proposed by Tumbull *et al.*[49] can well explain the appearance of 2-M ring. The stress concentration will appear in the part of the glass material and form shear bands, where the atoms move in a directed direction and enter into a smaller neighboring free-form void. That process will lead to the formation of 2-M ring.

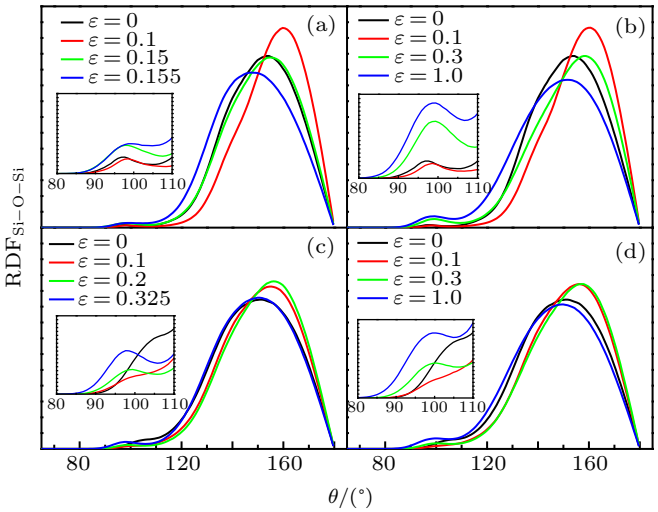


Fig. 8. The radial distribution function of Si–O–Si in S1 [(a), (b)] and S5 [(c), (d)] at the two strain rates [SR1: (a), (c); SR5: (b), (d)].

The variation of 3-fold Si, 4-fold Si, and 5-fold Si with strain is presented in Fig. 9. With the increase of strain, 5-fold Si gradually converts to 3-fold Si and 4-fold Si at SR1 [(a) and (b)]. When the fracture begins, 3-fold Si in S1 decreases rapidly but 3-fold Si in S5 still increases until the plastic flow stage ends. At the high strain rate of SR5 [(c) and (d)], we find

the plastic flow stage in all samples and 3-fold Si increases over the fracture strain, which becomes a same value for the all the samples. Differently, when the fracture begins, 4-fold Si is found to decrease and converts to 3-fold Si, too. It is shown that the conversion between coordinated silicon is dependent on both the densification and strain rate. As the fraction of coordinated silicon increases, the coordinated silicon will form atomic clusters. The atomic clusters can be rearranged to dissipate the energy of the bond around the matrix and the ability is related to the atomic density of the clusters.

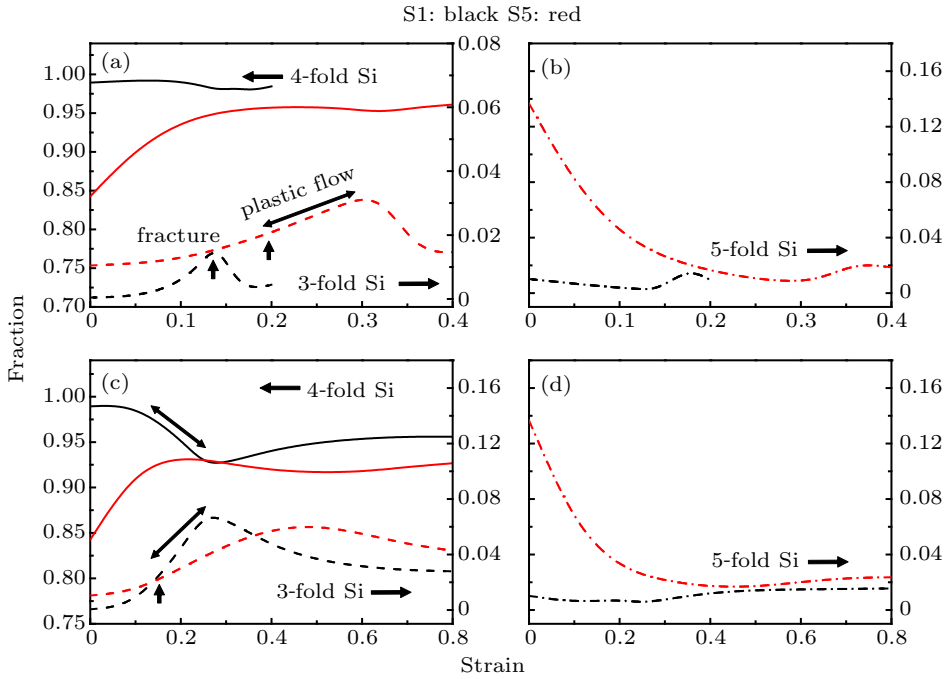


Fig. 9. Fraction of 3-fold Si, 4-fold Si, and 5-fold Si atoms as a function of strain at the two strain rates [SR1: (a), (b); SR5: (c), (d)].

4. Conclusion

In this work, we conducted MD simulations to investigate the fracture behavior of densified silica glass and its dependence on the strain rate. Firstly, the stress analysis indicates a quadratic reduction of tensile strength with the initial density. As for the same densified sample, the tensile strength increase with strain rate follows a power law, but the exponent will increase with the initial density of the sample. Besides, the fracture strain and strain energy exhibit a rapid increase over a certain densification, but fracture strain tends to the same value and strain energy becomes closer at extreme high strain rate.

The microstructural deformation suggests the transition from few cracks to a large area of damage in all the samples with the increase of strain rate. Strikingly, an evident plastic flow in the high densified sample appears, which reduces the tensile strength of densified sample and also results in the reduction of cracks relative the normal sample at higher strain rate. Furthermore, the RDF and ADF analyses show that both the Si–Si length and the Si–O–Si angle undergo expansion before fracture and contraction after fracture, and the formation of 2-M ring. The initial densification will weaken the expansion of bond length and angle. Further analysis of the coordinated silicon shows that the appearance of plastic flow is corresponding to the transition from 4-fold Si to 3-fold Si at high strain rate tension.

References

[1] Schuh C A, Hufnagel T C and Ramamurty U 2007 *Acta Mater.* **55** 4067
[2] Kumar G, Tang H X and Schroers J 2009 *Nature* **457** 868
[3] Telford M 2004 *Mater. Today* **7** 18
[4] Inoue A 2005 *P. Jpn. Acad. B-Phys.* **81** 156
[5] Chen Y C, Lu Z, Nomura K I, Wang W, Kalia R K, Nakano A and Vashishta P 2007 *Phys. Rev. Lett.* **99** 155506
[6] Irwin G 1957 *J. Appl. Mech.* **24** 351
[7] Barenblatt G I 1962 *Adv. Appl. Mech.* **7** 55
[8] Guin J P and Wiederhorn S M 2004 *Phys. Rev. Lett.* **92** 215502
[9] Bonamy D, Prades S, Rountree C L, Ponson L, Dalmas D, Bouchaud E, Ravi-Chandar K and Guillot C 2006 *Int. J. Fract.* **140** 3
[10] López-Cepero J M, Wiederhorn S M, Fett T and Guin J P 2007 *Int. J. Mater. Res.* **98** 1170
[11] Haile J M, Johnston I, Mallinckrodt A J and McKay S 1993 *Comput. Phys.* **7** 625
[12] Muralidharan K, Simmons J H, Deymier P A and Runge K 2005 *J. Non-Cryst. Solids* **351** 1532
[13] Muralidharan K, Oh K D, Deymier P A, Runge, K and Simmons J H 2007 *J. Mater. Sci.* **42** 4159
[14] Rimsza J M, Jones R E and Criscenti L J 2018 *J. Am. Ceram. Soc.* **101** 1488
[15] Jones R E and Zimmerman J A 2010 *J. Mech. Phys. Solids* **58** 1318
[16] Pedone A, Malavasi G, Menziani M C, Segre U and Cormack A N 2008 *Chem. Mat.* **20** 4356
[17] Vollmayr K, Kob W and Binder K 1996 *Phys. Rev. B* **54** 15808
[18] Ashwin J, Bouchbinder E and Procaccia I 2013 *Phys. Rev. E* **87** 042310
[19] Yuan F and Huang L 2012 *J. Non-Cryst. Solids* **358** 3481
[20] Wang J, Rajendran A M and Dongare A M 2015 *J. Mater. Sci.* **50** 8128
[21] Shi Y, Luo J, Yuan F and Huang L 2014 *J. Appl. Phys.* **115** 043528

[22] Chowdhury S C, Haque B Z and Gillespie J W 2016 *J. Mater. Sci.* **51** 10139
[23] Swiler T P, Simmons J H, Wright A C 1995 *J. Non-Cryst. Solids* **182** 68
[24] Ebrahem F, Bamer F and Markert B 2018 *Comput. Mater. Sci.* **149** 162
[25] Zhang F J, Zhou B H, Liu X, Song Y and Zuo X 2020 *Chin. Phys. B* **29** 027101
[26] Yuan F and Huang L 2014 *Sci. Rep.* **4** 1
[27] Lacks D J 1998 *Phys. Rev. Lett.* **80** 5385
[28] Liang Y, Miranda C R and Scandolo S 2007 *Phys. Rev. B* **75** 024205
[29] Hong N V, Vinh L T, Hung P K, Dung M V and Yen N V 2019 *Eur. Phys. J. B* **92** 183
[30] Hung P K, Vinh L T, Ha N T, Trang G T T and Hong N V 2020 *J. Non-Cryst. Solids* **530** 119780
[31] Le V V and Nguyen G T 2019 *J. Non-Cryst. Solids* **505** 225
[32] Le V V and Nguyen G T 2019 *Comput. Mater. Sci.* **159** 385
[33] Afify N D, Mountjoy G and Haworth R 2017 *Comput. Mater. Sci.* **128** 75
[34] Cowen B J and El-Genk M S 2015 *Comput. Mater. Sci.* **107** 88
[35] Barmes F, Soulard L and Mareschal M 2006 *Phys. Rev. B* **73** 224108
[36] Plimpton S 1995 *J. Comput. Phys.* **117** 1
[37] Tsai D H 1979 *J. Chem. Phys.* **70** 1375
[38] Subramaniyan A K and Sun C T 2008 *Int. J. Solids Struct.* **45** 4340
[39] Zhou H F, Zhong C, Cao Q P, Qu S X, Wang X D, Yang, W and Jiang J Z 2014 *Acta Mater.* **68** 32
[40] Sha Z, Wong W H, Pei Q, Branicio P S, Liu Z, Wang T, Guo T and Gao H 2017 *J. Mech. Phys. Solids* **104** 84
[41] Shimizu F, Ogata S and Li J 2007 *Mater. Trans.* **48** 2923
[42] Stukowski A 2009 *Model. Simul. Mater. Sci. Eng.* **18** 015012
[43] Smith WA and Michalske TM 1990 US-DOE Contract DEAC04-0DPOO789
[44] Argon A S 1979 *Acta Metall.* **27** 47
[45] Johnson W L and Samwer K 2005 *Phys. Rev. Lett.* **95** 195501
[46] Stein, G. D. 1979 *The Physics Teacher* **17** 503
[47] Bjornholm S 1990 *Contemp. Phys.* **31** 309
[48] Castleman A W and Jena P 2006 *Proc. Natl. Acad. Sci. USA* **103** 10552
[49] Polk D E and Tumbull D 1972 *Acta Metall.* **20** 493